Research Square

Preprints are preliminary reports that have not undergone peer review.
They should not be considered conclusive, used to inform clinical practice,
or referenced by the media as validated information.

Antimycobacterial activity and preliminary characterization of a 2-thio-malonylurea derivative against clinically relevant Mycobacterium species

Patrícia Cordeiro Moreira
Federal University of Goiás (UFG)
Antônio Silva Machado
Federal University of Goiás (UFG)
Vinícius Silva Pinto
Federal Institute of Goiano (IF Goiano)
Luciano Morais Lião
Federal University of Goiás (UFG)
Beatriz Santos Gontijo
Federal University of Goiás (UFG)
José Rodrigues do Carmo Neto
Federal University of Goiás (UFG)
Jonathas Xavier Pereira
Federal University of Goiás (UFG)
Glaura Regina Caldo Lima
Central Public Health Laboratory of the Federal District (LACEN-DF)
Maria Micaela Rodrigues Pereira
Federal University of Goiás (UFG)
André Kipnis
Federal University of Goiás (UFG)
Ieda Maria Sapateiro Torres
Federal University of Goiás (UFG)
Yasmin Castillos Ibrahim das Neves
Federal University of Rio Grande (FURG), Rio Grande – RS
Ana Júlia Reis
Federal University of Rio Grande (FURG), Rio Grande – RS
Pedro Eduardo Almeida Silva
Federal University of Rio Grande (FURG), Rio Grande – RS
Ricardo Menegatti
Federal University of Goiás (UFG)

Tracy Martina Marques Martins

tracy_martina@ufpa.br

Federal University of Pará (UFPA)

Research Article

Keywords: thiobarbituric acid, LQFM238, antimycobacterial activity, Mycobacterium spp., non-tuberculous mycobacteria, cytotoxicity

Posted Date: October 30th, 2026

DOI: https://doi.org/10.21203/rs.3.rs-11341655/v1

License: This work is licensed under a Creative Commons Attribution 4.0 International License. Read Full License

Additional Declarations: No competing interests reported.

Abstract

Mycobacterial infections remain a significant public health concern, particularly those caused by environmental and non-tuberculous mycobacteria (NTM). This study aimed to design, synthesize **2–11**, and evaluate 2-thio-malonylurea compounds as potential antimycobacterial agents. The synthesized compounds were subjected to *in silico* evaluation using SwissADME and screened for antibacterial activity against Gram-positive bacteria. The most active derivative was subsequently evaluated against clinically relevant *Mycobacterium* species, and its effects on mycobacterial morphology and mammalian cell viability were investigated by scanning electron microscopy (SEM) and cytotoxicity assays, respectively. LQFM238 (**7**) exhibited the strongest antibacterial activity among the compounds tested, showing activity against both Gram-positive bacterial species, with MIC values of 125 µg/mL against *S. aureus* and 250 µg/mL against *E. faecalis*. It showed antimycobacterial activity against *M. tuberculosis* H37Ra (MIC 62.5 µg/mL), *M. avium* (MIC 25 µg/mL), *M. abscessus* subsp. *bolletii* (MIC 50 µg/mL), and *M. abscessus* subsp. *abscessus* (MIC 50 µg/mL), whereas MIC value ≥ 100 µg/mL were observed for *M. intracellulare*. SEM revealed marked morphological alterations after exposure to 500 µg/mL for 24 h. Cytotoxic effects were observed only at 41.67 µg/mL, with selectivity indices of 4.15 for *M. avium* and 2.08 for both *M. abscessus* strains. LQFM238 (**7**) demonstrated promising antimycobacterial activity, particularly against *M. avium* and clinical *M. abscessus* strains.

1. Introduction

Infectious diseases remain a major challenge to global health, especially that caused by mycobacteria, which have become an increasing public health concern. These environmental mycobacteria are opportunistic pathogens capable of causing pulmonary disease, skin infections, and disseminated infections, particularly in immunocompromised individuals. The high mortality associated with these infections—particularly lower respiratory tract infections, skin infections, bloodstream infections and tuberculosis—combined with the escalating threat of antimicrobial resistance (AMR), underscores the urgent need for the research and development of new antimicrobial drugs. The emergence of multidrug-resistant bacterial pathogens has significantly limited the effectiveness of existing therapies, highlighting the importance of identifying novel chemical scaffolds with improved antimicrobial activity and safety profile (Ikuta et al. 2022; Murray et al. 2022; Langford et al. 2023; Wang et al. 2026).

Thio-malonylurea or thiobarbituric acid compounds have attracted considerable attention in medicinal chemistry due to their structural versatility and broad spectrum of biological activities. This heterocyclic scaffold allows extensive structural modification through substitution at distinct positions, enabling the fine-tuning of physicochemical and pharmacological properties. Several studies have reported that thiobarbituric acid compounds exhibit diverse biological activities, including antimicrobial, antiviral, antioxidant, and anticancer effects (Dabholkar and Ravi 2010; Jin et al. 2012; McKinnie et al. 2014; Elshaier et al. 2016; Sharma et al. 2018). These pharmacological profile highlight thiobarbituric acid scaffold as lead compounds for the research and development of new antimicrobial agents (Kaur et al. 2014; Elshaier et al. 2016).

Therefore, this study aimed to design, synthesize, and evaluate a series of 2-thio-malonylurea compounds which were assessed against bacterial. The compounds **2–11** were initially subjected to *in silico* assessment, of their physicochemical and pharmacokinetic properties using SwissADME, followed by biological screening against Gram-positive bacteria. The best compound LQFM238 (**7**) was evaluated against clinically relevant *Mycobacterium* species. The mycobacterial morphology exposed to LQFM238 (**7**) was further investigated by scanning electron microscopy (SEM), and while their cytotoxicity was assessed in mammalian cells.

2. Materials and Methods

2.1. Chemistry

General

Reaction progress was monitored using thin-layer chromatography (TLC) on commercially available pre-coated silica plates (Whatman 60 F254), and plates were visualized using UV light at 254 nm and 365 nm. ^{1}H and ^{13}C-NMR spectra were recorded on a Bruker Avance III 500 MHz spectrometer in the indicated solvent. All chemical shifts are referenced to TMS in ppm, while coupling constants are presented in Hertz. All assignments in the signals of ^{1}H and ^{13}C NMR spectra were consistent with the proposed chemical structures. Infrared (IR) spectra were obtained on a Perkin-Elmer Spectrum Bx-II FT-IR spectrophotometer using KBr discs. Melting points were determined using a Marte apparatus and are presented as uncorrected. Organic solutions were dried over anhydrous sodium sulfate, and the solvents were removed under reduced pressure employing a rotary evaporator. For mass spectrometry analyses, samples were prepared by dissolving 1.0 µg of each compound in 1.0 mL of methanol. High-resolution mass spectrometry (HRMS) was performed using a Bruker microTOF III instrument (Bruker Daltonics, Bremen, Germany). Samples were introduced into the ESI source at a flow rate of 5 µL/min. The ESI (+) source parameters were set as follows: nitrogen nebulizer at 0.4 Bar, capillary voltage 4500 V, transfer capillary temperature 200°C, dry gas flow 4.0 L/min, end plate offset 500 V. Mass spectra were recorded and analyzed using Compass Data Analysis software (Bruker Daltonics, Bremen, Germany).

2.1.1. General Procedure (Lou et al. 2010): To a mixt mixture of H_2O/EtOH 50% (10 mL, v/v) were aldehydes (**32–41**) (1 mmol) and 2-thioxo-dihydropyrimidine-4,6(1H,5H)-dione (**42**) (144 mg, 1.00 mmol) and the reaction mixture was maintained at 80°C for 4 hours. At the end of the reaction, the precipitate was filtered off and was washed 1x30 mL with warm H_2O, EtOH and CH_2Cl_2, to render compounds **2–11**.
2.1.1.1. Synthesis of 5-((1-phenyl-1H-pyrazol-4-yl)methylene)-2-thioxo-dihydropyrimidine-4,6(1H,5H)-dione (2) (LQFM231): compound (**2**) was obtained in 63% of yield, as a yellow solid, m.p.= > 230ºC ºC, Rf = 0.40 (CH_2Cl_2:MeOH 95:5). IR_{max} (KBr) cm^{-1}: 3435 (v N-H); 3144 (v C-H); 1707 (v C = S); 1673 (v C = O) and 1567 (v C = C); ^{1}H-NMR (500.13 MHz) DMSO-d_6/TMS (δ): 12.43 (1H, *s*, H3”), 12.41 (1H, *s*, H5”), 9.56 (1H, *s*, H5), 8.85 (1H, *s*, H3), 8.35 (1H, *s*, H6), 7.89 (2H, *ddd*, *J* = 8.6, 2.1 and 1.2 Hz, H2’ and 6’); 7.59 (2H, *ddd*, *J* = 8.6, 7.4 and 2.1 Hz, H3’ and 5’), 7.45 (1H, *tt*, *J* = 7.4 and 1.2 Hz, H4’); 2D NMR

(HSQC/HMBC-125.76 MHz) DMSO-d_6/TMS (δ): 178.4 (C-4”), 161.9 and 160.7 (C-2” and 6”), 146.9 (C-3), 144.6 (C-6), 138.5 (C-1’), 136.0 (C-5), 129.7 (C-3’ and 5’), 127.8 (C-4’), 119.2 (C-2’ and 6’), 119.0 (C-4), 114.1 (C-1”); ESI-MS calculated for $C_{14}H_{11}N_4O_2S$ $[M + H]^+$ m/z of 299.0603, found: 299.0606, Error= -5.4 ppm;

2.1.1.2. Synthesis of 5-((1-(4-fluorophenyl)-1H-pyrazol-4-yl)methylene)-2-thioxo-dihydropyrimidine-4,6(1H,5H)-dione (3) (LQFM232): compound (**3**) was obtained in 77% of yield, as an orange solid, m.p.= > 230ºC ºC, Rf = 0.62 (CH_2Cl_2:MeOH 95:5). IR_{max} (KBr) cm^{-1}: 3450 (v N-H); 3096 (v C-H); 1699 (v C = S); 1654 (v C = O) and 1566 (v C = C); ^{1}H-NMR (500.13 MHz) DMSO-d_6/TMS (δ): 12.43 (1H, *s*, H3”), 12.41 (1H, *s*, H5”), 9.50 (1H, *s*, H5), 8.83 (1H, *s*, H3), 8.33 (1H, *s*, H6), 7.92 (2H, *dd*, *J* = 8.6 and 4.7 Hz, H2’ and 6’), 7.44 (2H, *brt*, *J* = 8.6 Hz, H3’ and 5’); 2D NMR (HSQC/HMBC-125.76 MHz) DMSO-d_6/TMS (δ): 178.7 (C-4”), 162.5 and 161.1 (C-2” and 6”), 161.7 (C-4’), 147.0 (C-3), 144.6 (C-6), 136.3 (C-5), 135.6 (C-1’), 121.4 (C-2’ and 6’),119.4 (C-4), 116.5 (C-3’ and 5’), 114.5 (C-1”); ESI-MS calculated for $C_{14}H_{10}FN_4O_2S$ $[M + H]^+$ m/z of 317.0508, found: 317.0511, Error= -2.6 ppm;

2.1.1.3. Synthesis of 5-((1-(2-fluorophenyl)-1H-pyrazol-4-yl)methylene)-2-thioxo-dihydropyrimidine-4,6(1H,5H)-dione (4) (LQFM233): compound (**4**) was obtained in 69% of yield, as a brown solid, m.p.= > 230ºC ºC, Rf = 0.44 (CH_2Cl_2:MeOH 95:5). IR_{max} (KBr) cm^{-1}: 3455 (v N-H); 3068 (v C-H); 1707 (v C = S); 1655 (v C = O) and 1567 (v C = C); ^{1}H-NMR (500.13 MHz) DMSO-d_6/TMS (δ): 12.44 (1H, *s*, H3”), 12.41 (1H, *s*, H5”), 9.49 (1H, *d*, *J* = 2.1 Hz, H5), 8.80 (1H, *s*, H3), 8.39 (1H, *s*, H6), 7.92 (2H, *td*, *J* = 8.1 and 1.3 Hz, H5’), 7.61–7.49 (2H, *m*, H4’ and 6’), 7.43 (1H, *ddd*, *J* = 8.4, 5.7 and 2.4 Hz, H3’); 2D NMR (HSQC/HMBC-125.76 MHz) DMSO-d_6/TMS (δ): 178.8 (C-4”), 162.5 and 161.7 (C-2” and 6”), 153.8 (C-2’), 147.9 (C-3), 145.5 (C-5), 139.8 (C-5), 130.6 (C-4’), 127.3 (C-1’), 126.1 (C-3’), 125.5 (C-5’), 119.3 (C-4), 117.7 (C-6’), 114.9 (C-1”); ESI-MS calculated for $C_{14}H_{10}FN_4O_2S$ $[M + H]^+$ m/z of 317.0508, found: 317.0527, Error= -6.9 ppm;

2.1.1.4. Synthesis of 5-((1-(4-chlorophenyl)-1H-pyrazol-4-yl)methylene)-2-thioxo-dihydropyrimidine-4,6(1H,5H)-dione (5) (LQFM234): compound (**5**) was obtained in 81% of yield, as a yellow solid, m.p.= > 230ºC ºC, Rf = 0.79 (CH_2Cl_2:MeOH 95:5). IR_{max} (KBr) cm^{-1}: 3440 (v N-H); 3062 (v C-H); 1706 (v C = S); 1650 (v C = O) and 1567 (v C = C); ^{1}H-NMR (500.13 MHz) DMSO-d_6/TMS (δ): 12.44 (1H, *s*, H3”), 12.42 (1H, *s*, H5”), 9.56 (1H, *s*, H5), 8.85 (1H, *s*, H3), 8.33 (1H, *s*, H6), 7.92 (2H, d_{ab}, *J* = 8.9 Hz, H2’ and 6’), 7.66 (2H, d_{ab}, *J* = 8.9 Hz, H3’ and 5’); 2D NMR (HSQC/HMBC-125.76 MHz) DMSO-d_6/TMS (δ): 179.0 (C-4”), 162.2 and 161.2 (C-2” and 6”), 147.7 (C-3), 145.0 (C-6), 137.4 (C-1’), 136.9 (C-5), 132.9 (C-4’), 130.3 (C-3’ and 5’), 121.5 (C-2’ and 6’), 119.7 (C-4), 114.9 (C-1”); ESI-MS calculated for $C_{14}H_{10}ClN_4O_2S$ $[M + H]^+$ m/z of 333.0213, found: 333.0213, Error= -1.7 ppm;

2.1.1.5. Synthesis of 5-((1-(2-chlorophenyl)-1H-pyrazol-4-yl)methylene)-2-thioxo-dihydropyrimidine-4,6(1H,5H)-dione (6) (LQFM237): compound (**6**) was obtained in 45% of yield, as a yellow solid, m.p.= > 230ºC ºC, Rf = 0.68 (CH_2Cl_2:MeOH 95:5). IR_{max} (KBr) cm^{-1}: 3403 (v N-H); 3100 (v C-H); 1709 (v C = S);

1685 (v C = O) and 1574 (v C = C); ^{1}H-NMR (500.13 MHz) DMSO-d_6/TMS (δ): 12.44 (1H, *s*, H3”), 12.40 (1H, *s*, H5”), 9.37 (1H, *s*, H5), 8.79 (1H, *s*, H3), 8.38 (1H, *s*, H6), 7.79–7.75 (1H, *m*, H 6’), 7.75–7.71 (1H, *m*, H3’), 7.63–7.59 (1H, *m*, H5’), 7.59–7.55 (1H, *m*, H4’); 2D NMR (HSQC/HMBC-125.76 MHz) DMSO-d_6/TMS (δ): 178.7 (C-4”), 162.1 and 160.9 (C-2” and 6”), 147.3 (C-3), 145.2 (C-3), 141.1 (C-5), 137.1 (C-2’), 136.7 (C-1’), 131.0 (C-5’), 130.0 (C-6’), 127.6 (C-3’), 118.6 (C-4), 114.6 (C-1”); ESI-MS calculated for $C_{14}H_{10}ClN_4O_2S$ $[M + H]^+$ m/z of 333.0213, found: 333.0179, Error = 8.7 ppm;

2.1.1.6. Synthesis of 5-((1-(3-chlorophenyl)-1H-pyrazol-4-yl)methylene)-2-thioxo-dihydropyrimidine-4,6(1H,5H)-dione (7) **(LQFM238)**: compound (7) was obtained in 72% of yield, as a yellow solid, m.p.= > 230ºC ºC, Rf = 0.79 (CH_2Cl_2:MeOH 95:5). IR_{max} (KBr) cm^{-1}: 3438 (v N-H); 3082 (v C-H); 1705 (v C = S); 1652 (v C = O) and 1569 (v C = C); ^{1}H-NMR (500.13 MHz) DMSO-d_6/TMS (δ): 12.40 (1H, *s*, H3”), 12.38 (1H, *s*, H5”), 9.55 (1H, *s*, H5), 8.85 (1H, *s*, H3), 8.31 (1H, *s*, H6), 7.97 (1H, *t*, *J* = 2.1 Hz, H2’), 7.87 (1H, *ddd*, *J* = 8.1, 2.1 and 0.8 Hz, H6’), 7.61 (1H, *t*, *J* = 8.1 Hz, H5’), 7.50 (1H, *ddd*, *J* = 8.1, 2.1 and 0.8 Hz, H2’); 2D NMR (HSQC/HMBC-125.76 MHz) DMSO-d_6/TMS (δ): 178.8 (C-4”), 162.3 and 160.8 (C-2” and 6”), 147.7 (C-3), 144.8 (C-6), 139.9 (C-1’), 137.2 (C-5), 134.6 (C-3’), 134.2 (C-5’), 128.4 (C-4’), 119.7 (C-2’), 119.6 (C-4), 118.6 (C-6’), 114.8 (C-1”); ESI-MS calculated for $C_{14}H_{10}ClN_4O_2S$ $[M + H]^+$ m/z of 333.0213, found: 333.0220, Error= -3.6 ppm;

2.1.1.7. Synthesis of 5-((1-(2-bromophenyl)-1H-pyrazol-4-yl)methylene)-2-thioxo-dihydropyrimidine-4,6(1H,5H)-dione (8) (LQFM239): compound (**8**) was obtained in 56% of yield, as a beige solid, m.p.= > 230ºC ºC, Rf = 0.79 (CH_2Cl_2:MeOH 95:5). IR_{max} (KBr) cm^{-1}: 3439 (v N-H); 3068 (v C-H); 1707 (v C = S); 1650 (v C = O) and 1561 (v C = C); ^{1}H-NMR (500.13 MHz) DMSO-d_6/TMS (δ): 12.40 (1H, *s*, H3”), 12.37 (1H, *s*, H5”), 9.31 (1H, *s*, H5), 8.77 (1H, *s*, H3), 8.38 (1H, *s*, H6), 7.89 (1H, *dd*, *J* = 8.1 and 1.1 Hz, H3’), 7.68 (1H, *dd*, *J* = 7.9 and 1.4 Hz, H6’), 7.61 (1H, *ddd*, *J* = 7.9, 7.6 and 1.1 Hz, H5’), 7.52 (1H, *ddd*, *J* = 8.1, 7.6 and 1.4 Hz, H4’); 2D NMR (HSQC/HMBC-125.76 MHz) DMSO-d_6/TMS (δ): 178.7 (C-4”), 162.0 and 160.8 (C-2” and 6”), 147.7 (C-3), 145.8 (C-6), 141.4 (C-5), 138.8 (C-1’), 134.5 (C-3’), 132.2 (C-4’), 129.8 (C-5’), 129.4 (C-6’), 118.8 (C-2’), 118.6 (C-4), 114.5 (C-1”); ESI-MS calculated for $C_{14}H_{10}BrN_4O_2S$ $[M + H]^+$ m/z of 376.9708, found: 376.9692, Error= -3.1 ppm;

2.1.1.8. Synthesis of 5-((1-(3-fluorophenyl)-1H-pyrazol-4-yl)methylene)-2-thioxo-dihydropyrimidine-4,6(1H,5H)-dione (9) (LQFM240): compound (**9**) was obtained in 25% of yield, as a green solid, m.p.= > 230ºC ºC, Rf = 0.62 (CH_2Cl_2:MeOH 95:5). IR_{max} (KBr) cm^{-1}: 3430 (v N-H); 3067 (v C-H); 1709 (v C = S); 1671 (v C = O) and 1568 (v C = C); ^{1}H-NMR (500.13 MHz) DMSO-d_6/TMS (δ): 12.45 (1H, *s*, H3”), 12.43 (1H, *s*, H5”), 9.56 (1H, *s*, H5), 8.86 (1H, *s*, H3), 8.32 (1H, *s*, H6), 7.78 (1H, *ddd*, *J* = 10.2, 2.5 and 2.3 Hz, H2’), 7.76 (1H, *ddd*, *J* = 8.0, 2.3 and 0.9 Hz, H6’), 7.64 (1H, *ddd*, *J* = 8.3, 8.0 and 2.0 Hz, H5’), 7.30 (1H, *dddd*, *J* = 8.5, 8.3, 2.5 and 0.9 Hz, H4’); 2D NMR (HSQC/HMBC-125.76 MHz) DMSO-d_6/TMS (δ): 179.0 (C-4”), 162.6 and 161.2 (C-2” and 6”), 162.5 (C-3’), 148.1 (C-3), 145.4 (C-6), 140.5 (C-1’), 137.7 (C-5), 132.8 (C-5’), 119.9 (C-4), 116.2 (C-6’), 115.3 (C-1”), 107.8 (C-2’), ; ESI-MS calculated for $C_{14}H_{10}FN_4O_2S$ $[M + H]^+$ m/z of 317.0508, found: 317.0521, Error= -5.6 ppm;

2.1.1.9. Synthesis of 5-((1-(3-bromophenyl)-1H-pyrazol-4-yl)methylene)-2-thioxo-dihydropyrimidine-4,6(1H,5H)-dione (10) (LQFM281): compound (**10**) was obtained in 75% of yield, as a yellow solid, m.p.= > 230ºC ºC, Rf = 0.52 (CH_2Cl_2:MeOH 95:5). IR_{max} (KBr) cm^{-1}: 3433 (v N-H); 3074 (v C-H); 1705 (v C = S); 1652 (v C = O) and 1571 (v C = C); ^{1}H-NMR (500.13 MHz) DMSO-d_6/TMS (δ): 12.41 (1H, *s*, H3”), 12.39 (1H, *s*, H5”), 9.56 (1H, *s*, H5), 8.85 (1H, *s*, H3), 8.31 (1H, *s*, H6), 8.11 (1H, *dd*, *J* = 2.1 and 2.0 Hz, H2’), 7.91 (1H, *ddd*, *J* = 8.1, 2.0 and 1.9 Hz, H6’), 7.64 (1H, *ddd*, *J* = 8.0, 2.1 and 1.9 Hz, H4’), 7.54 (1H, *dd*, *J* = 8.1 and 8.0 Hz, H4’); 2D NMR (HSQC/HMBC-125.76 MHz) DMSO-d_6/TMS (δ): 178.4 (C-4”), 161.8 and 160.4 (C-2” and 6”), 147.1 (C-3), 144.4 (C-6), 139.6 (C-1’), 136.7 (C-5), 131.8 (C-5’), 130.6 (C-4’), 122.4 (C-2’), 121.9 (C-3’), 119.2 (C-4), 118.3 (C-6’), 114.5 (C-1”); ESI-MS calculated for $C_{14}H_{10}BrN_4O_2S$ $[M + H]^+$ m/z of 376.9708, found: 376.9588, Error = 10.7 ppm;

2.1.1.10. Synthesis of 5-((1-(4-bromophenyl)-1H-pyrazol-4-yl)methylene)-2-thioxo-dihydropyrimidine-4,6(1H,5H)-dione (11) (LQFM282): compound (**11**) was obtained in 21% of yield, as an orange solid, m.p.= > 230ºC ºC, Rf = 0.60 (CH_2Cl_2:MeOH 95:5). IR_{max} (KBr) cm^{-1}: 3434 (v N-H); 3061 (v C-H); 1705 (v C = S); 1650 (v C = O) and 1568 (v C = C); ^{1}H-NMR (500.13 MHz) DMSO-d_6/TMS (δ): 12.41 (1H, *s*, H3”), 12.39 (1H, *s*, H5”), 9.55 (1H, *s*, H5), 8.84 (1H, *s*, H3), 8.32 (1H, *s*, H6), 7.85 (2H, d_{ab}, *J* = 9.0 Hz, H2’ and 6’), 7.78 (2H, d_{ab}, *J* = 9.0 Hz, H2’ and 6’); 2D NMR (HSQC/HMBC-125.76 MHz) DMSO-d_6/TMS (δ): 178.4 (C-4”), 161.5 and 161.1 (C-2” and 6”), 147.2 (C-3), 144.2 (C-6), 137.6 (C-1’), 136.3 (C-5), 132.9 (C-3’ and 5’), 121.2 (C-2’ and 6’), 120.3 (C-4’), 119.1 (C-4), 114.3 (C-1”); ESI-MS calculated for $C_{14}H_{10}BrN_4O_2S$ $[M + H]^+$ m/z of 376.9708, found: 376.9692, Error= -3.1 ppm;

2.2. *In silico* assay

The 2-tio-malonilureia compounds **2–11** were evaluated through *in silico* prediction of physicochemical: properties molecular weight and estimation of molar refractivity by Crippen's fragmentation with ChemBioDraw. SwissADME is used for evaluation of fragmentation topological polar surface area (TPSA), lipophilicity and consensus Log $P_{o/w}$ (consensus obeyed average iLOGP1.5; XLOGP3; WLOGP; MLOGP and SILICOS-IT). The water solubility was description on evaluation of Log S (ESOL); with pharmacokinetics GI absorption, BBB permeant, P-gp substrate and Log K_P (skin permeation). Additionally, it was described as Druglikeness, with Lipinski and bioavailability Score.

2.3. Biological screening against bacterial cells

All 2-thio-malonylurea compounds **2–11** were initially screened for antibacterial activity against Gram-positive bacteria using the broth microdilution method. The minimum inhibitory concentrations (MICs) were determined against *Staphylococcus aureus* ATCC 6538 and *Enterococcus faecalis* ATCC 29212 in 96-well microtiter plates, in duplicate, according to a standard broth microdilution protocol (NCCLS 2003; Wiegand et al. 2008; Guo et al. 2020). The test compounds were initially solubilized in 1 mL of dimethyl sulfoxide (DMSO) and subsequently diluted in 9 mL of Mueller-Hinton (MH) broth to obtain a stock

solution. In sterile 96-well microplates, 200 µL of each compound at a concentration of 1000 µg/mL were added to wells in the first column. Each plate evaluated three compounds (rows A–F). Using a multichannel pipette, a twofold serial dilution was conducted across columns 1 to 10 by transferring 100 µL from one well to the adjacent well containing 100 µL of MH broth. This resulted in a two-fold serial dilution series ranging from 1000 to 1.95 µg/mL. Ciprofloxacin (25 µg/mL) was used as a positive control against bacteria (row G), while 10% DMSO (v/v) served as the negative control (row H). Columns 11 and 12 were reserved for sterility control and bacterial growth control, respectively. The bacterial inoculum was adjusted to an optical density of 0.08–0.1 at 625 nm (equivalent to 0.8–1 × 10^8 CFU/mL), then diluted 1:10 in saline. Each test received well received 5 µL of inoculum in 100 µL of broth, resulting in a final bacterial concentration of 5 × 10^5 CFU/mL per well). Plates were covered and incubated at 35 ± 2°C for 20–22 hours. After incubation, 20 µL of 0.5% triphenyl tetrazolium chloride (TTC) was added to each well, followed by an additional 45 minutes of incubation. A red color indicated bacterial growth. The MIC was defined as the lowest compound concentration that prevented visible growth (no red coloration).

2.4. Antibacterial activity and determination of MIC and MBC in *Mycobacterium* Species

Among the compounds **2–11** evaluated in the screening, just LQFM238 (**7**) demonstrated antibacterial activity against both bacteria cells. Therefore, it was selected for further evaluation against *Mycobacterium* species and assessed in duplicate to determine its MIC and minimum bactericidal concentration (MBC), all experiments (MIC and MBC) were conducted in triplicate. MIC assays determine against *Mycobacterium tuberculosis* H37Ra (ATCC 25177, avirulent), and clinical strains of *Mycobacterium avium* and *Mycobacterium intracellulare* were subsequently performed using the broth microdilution method in 96-well microplates.

Each plate included appropriate controls: wells containing only culture broth served as negative controls, whereas wells containing the respective antibiotics served as positive controls (Martin et al. 2003; Wiegand et al. 2008; Clinical and Laboratory Standards Institute (CLSI) 2018). A stock solution of LQFM238 (**7**) was prepared by dissolving 20 mg of compound in 1 mL of DMSO, followed by dilution in 9 mL of phosphate-buffered saline (PBS). Serial dilutions were then conducted in sterile 96-well microplates containing Mueller-Hinton Broth (MH).

Mycobacterial growth of *M. tuberculosis* H37Ra was assessed using resazurin as a colorimetric indicator of cell viability (Palomino et al. 2002; Martin et al. 2003; Ramis et al. 2015). The microdilution method using sterile Middlebrook 7H9 broth supplemented with 0.01% resazurin. In sterile 96-well microplates, 200 µL of the test compound—previously diluted to a concentration of 2000 µg/mL—was added to the first well of each row. Serial two-fold dilutions were then performed across the wells, yielding a final concentration range from 2000 µg/mL to 0.00024 µg/mL, totaling twenty-four tested concentrations.

The *M. tuberculosis* H37Ra inoculum was standardized according to McFarland at a concentration of 1.0x10^8 CFU/mL. This inoculum was diluted 1:25 in sterile distilled water. The same inoculum used in

the microdilution assay was prepared in sterile Middlebrook 7H9 broth. Rifampicin was included as the positive antibiotic control, while 10% (v/v) DMSO was used as the negative control. Sterility controls for the culture medium and mycobacterial growth control were also included. The plates were sealed with plastic film and incubated at 37°C in a humidified incubator for 7 days. After 5–6 days of incubation, 20 µL of resazurin solution (100 µg/mL, 0.01%) was added to the control wells, followed by an additional 18–24 hours of incubation at 37°C to allow for color development. A pink coloration indicated viable mycobacterial growth, while a blue coloration indicated loss of viability. The MIC was defined as the lowest concentration of the tested compound that resulted in a blue color, indicating complete inhibition of bacterial growth.

Only LQFM238 (**7**) was also assessed against four clinical strains of non-tuberculous mycobacteria (NTM): *Mycobacterium abscessus* subsp. *bolletii*, *M. abscessus* subsp. *abscessus*. The MIC values were determined using the broth microdilution method in 96-well microplates, following the protocols described by Palomino et al. 2002 and the CLSI, 2018. Mycobacterial growth was assessed using resazurin as a colorimetric indicator of cell viability (Palomino et al. 2002; Martin et al. 2003; Ramis et al. 2015; Clinical and Laboratory Standards Institute (CLSI) 2018). The MIC was defined as the lowest concentration of the LQFM238 (**7**) that resulted in complete inhibition of visible bacterial growth. Each assay included appropriate negative and positive controls.

The MBC evaluated against the clinical strain *M. abscessus* subsp. *massiliense* GO06 (Raiol et al. 2012; Das Neves et al. 2019). The bacterial concentration was measured using a spectrophotometer at 590 nm, where 1 OD of *M. abscessus* subsp. *massiliense* GO06 corresponds to 1×10^8 CFU/mL. The inoculum was adjusted in Mueller-Hinton broth to 2×10^3 CFU/mL. Clarithromycin (10% w/v) was used as a positive control, DMSO (10% v/v) as a negative control, and sterility and growth controls were included. Antimicrobial activity of the LQFM238 (**7**) was assessed by serial dilutions ranging from 1000 to 15.63 µg/mL. After 24 h incubation, wells were diluted 1:10, and 50 µL of each dilution was plated on Mueller-Hinton agar. For the highest concentrations (1000–31.25 µg/mL), select wells were further serially diluted prior to plating on 7H11/OADC agar (Raiol et al. 2012; Oliveira et al. 2018).

The Petri dishes were incubated at 35°C ± 2°C for 5 days. After the incubation time, colonies were counted. The count was conducted on the three plates, from triplicate experiments, and the absolute values of each count are expressed. Sequentially, the mean, standard deviation and percentage of the count found were performed. The MBC was determined as the lowest concentration that completely inhibited mycobacterial growth.

2.5. Sample preparation and imaging in scanning electron microscopy

Colonies of *M. abscessus* subsp. *massiliense* GO06, grown on nutrient agar during incubation in 35°C ± 2°C for 5 days, and either treated or untreated with LQFM238 (**7**) compound, were examined using scanning electron microscopy (SEM). For the treatment, LQFM238 (**7**) was diluted in broth to a concentration below the MIC, following a modified protocol adapted from Das Neves et al. 2019 and

Martins et al. 2025 (Das Neves et al. 2019; Martins et al. 2025). Three samples were prepared for analysis: one untreated colony (control) and two colonies exposed to 500 µg/mL of LQFM238 (**7**) for 24 hours. Following incubation, the compound was removed, and the samples were fixed in Karnovsky's fixative containing sodium cacodylate buffer, for 30 minutes at 4°C. After fixation, the samples underwent serial dehydration for 10 minutes, subsequently, the samples were treated with acetone and then hexamethyldisilazane (HMDS) for a further 300 seconds. The dehydrated colonies were coated with a thin layer of gold using a Denton Vacuum Desk V sputter coater. Imaging was performed on a JEOL JSM-7100F Field Emission Scanning Electron Microscope (FEG-SEM) at an accelerating voltage of 3 kV, employing the Secondary Electron Detection (SED) mode.

2.6. Cellular viability

2.6.1. Cytotoxicity Assay Preparation

For the evaluation of cytotoxicity, 1 mg of LQFM238 (**7**) was dissolved in 480 µL of DMSO. Subsequently, 23.52 µL of unsupplemented RPMI medium was added, yielding a stock solution with a maximum DMSO concentration of 2% and a final LQFM238 (**7**) concentration of 0.042 mg/mL. From this stock, five serial concentrations were prepared for testing.

2.6.2. Cell Culture

The study employed the L929 fibroblast cell line of murine origin, acquired from the Rio de Janeiro Cell Bank (BCRJ, Rio de Janeiro, RJ, Brazil). Cells were maintained in Gibco Roswell Park Memorial Institute (RPMI) 1640 medium, supplemented with 5% fetal bovine serum (FBS) and 0.01% penicillin/streptomycin. Cultures were grown in 75 cm^2 flasks at 37°C within a humidified incubator containing 5% CO_2 and 95% air. Before experimentation, cells were rinsed with PBS, detached using a 0.25/0.03% EDTA solution, and centrifuged at 1000 rpm for 5 minutes. The supernatant was removed, and the resulting cell pellet was resuspended in fresh culture medium for subsequent cell counting.

2.6.3. Cytotoxicity Assay Procedure

L929 cells were plated in 24-well plates at a density of 1×10^5 cells per well in 1000 µL of supplemented medium and incubated for 24 hours to permit cell attachment. After this incubation period, the culture medium was removed and replaced with the test solution. In the first set of four wells, 1 mL of the test solution was applied. For each successive set of four wells, the volume of the test solution was reduced by half and topped up with unsupplemented RPMI medium to ensure a consistent final volume. After adding the test solution and the positive control, the cells were incubated under standard culture conditions (37°C, 5% CO_2, humidified atmosphere) for 24 hours. After incubation, cells were observed using an inverted microscope, then washed with sterile PBS and incubated for 20 minutes with 1000 µL of PBS containing 6 µL of neutral red dye. The PBS was then removed and replaced. Next, 3.5 µL of Evans Blue dye was added to each well, and the cells were incubated for a further 20 minutes. Following the second staining step, the dye-containing PBS was discarded and replaced with fresh PBS. Images

were then captured at 200× magnification using an inverted microscope. Cell viability was quantified using TMArker software, previously trained to differentiate between live and dead cells.

2.6.4. Statistical Analysis

GraphPad Prism 8 software was employed for both statistical analysis and the creation of graphs for cell viability measurements. Data normality was first evaluated using the Shapiro-Wilk test. Differences between groups were subsequently assessed by ordinary one-way ANOVA. The cytotoxic concentration causing 50% cell death (CC50) was determined through nonlinear regression analysis and is reported as mean ± standard deviation. Statistical significance was defined as $p < 0.05$.

2.7. Selectivity index (SI)

The selectivity index (SI) was calculated as the ratio of CC_{50} to the MIC ($SI = CC_{50}/MIC$) for each mycobacterial strain. In antimicrobial drug discovery, SI values are commonly interpreted as follows: SI > 10 indicates high selectivity, SI 1–10 is considered acceptable for lead compounds, and SI < 1 is regarded as problematic (Repetto et al. 2008; Lamut et al. 2019)

3. Results

3.1. Synthesis

The first two synthetic steps were done using the same method described by Da Mota et al. 2018 and are shown in Fig. 1. In turn, the last step was carried out through Knoevenagel reaction to provide LQFM compounds **2–11** at global yields between 11 to 57% (Fig. 1B).

3.2. *In silico* assay

The physicochemical and pharmacokinetic properties of the compounds **2–11**, including molecular weight, estimation of molar refractivity (MR), topological polar surface area (TPSA), consensus lipophilicity (Consensus Log $P_{o/w}$), and water solubility, were evaluated. Consensus Log $P_{o/w}$ was calculated as the average of the values obtained using iLOGP, XLOGP3, WLOGP, MLOGP, and SILICOS-IT. Water solubility was estimated using the ESOL (Estimated Solubility) model. The results are presented in Table 1.

Table 1
In silico assay of compounds **2–11**.

W	Compound	Molecular weight g/mol[a]	MR cm^3/mol[a]	Log $P_{o/w}$ (consensus)[b]	Log S (ESOL) [b]	Log K_P (skin permeation)[b] cm/s
H	LQFM231 (**2**)	298.32	81,20	0.88	-2.91 Soluble	-7.03
2Br	LQFM239 (**8**)	377.22	88,89	1.69	-3.82 Soluble	-7.02
2Cl	LQFM237 (**6**)	332.76	85,81	1.59	-3.50 Soluble	-6.80
2F	LQFM233 (**4**)	316.31	81,61	1.38	-3.07 Soluble	-7.07
3Br	LQFM281 (**10**)	377.22	88,89	1.72	-3.82 Soluble	-7.02
3Cl	LQFM238 (**7**)	332.76	85,81	1.64	-3.50 Soluble	-6.80
3F	LQFM240 (**9**)	316.31	81,61	1.40	-3.07 Soluble	-7.07
4Br	LQFM282 (**11**)	377.22	88,89	1.73	-3.82 Soluble	-7.02
4Cl	LQFM234 (**5**)	332.76	85,81	1.65	-3.50 Soluble	-6.80
4F	LQFM232 (**3**)	316.31	81,61	1.44	-3.07 Soluble	-7.07

ChemBioDraw[a]; SwissADME[b].

In prediction model of SwissADME all compounds exhibited a TPSA of 108.11 Å², no Lipinski rule-of-five violations, and a bioavailability score of 0.55. The compounds showed high gastrointestinal (GI)

absorption, were predicted to be non-BBB permeant, and were not predicted to be substrates of P-glycoprotein (P-gp). In addition, all compounds have a potential inhibitory activity against CYP1A2.

3.3. Biological screening against bacterial cells

The 2-thio-malonylurea compounds (**2–11**) were evaluated for antibacterial activity against Gram-positive bacterial cells, and the results of the antibacterial screening are presented in Table 2. Among the compounds assessed, compound LQFM238 (**7**) exhibited the most pronounced antibacterial activity active against both *S. aureus* ATCC 6538 and *E. faecalis* ATCC 29212. The observed inhibition of both Gram-positive bacteria supported the selection of this derivative for further investigation against antimycobacterial.

Table 2
Biological screening against Gram-positive bacterial cells of compounds **2–11**.

Compound	**MIC** ***S. aureus*** **ATCC 6538**	**MIC** ***E. faecalis*** **ATCC 29212**
LQFM231 (**2**)	250 µg/mL	-
LQFM232 (**3**)	250 µg/mL	-
LQFM233 (**4**)	250 µg/mL	-
LQFM234 (**5**)	250 µg/mL	-
LQFM237 (**6**)	250 µg/mL	-
LQFM238 (**7**)	125 µg/mL	250 µg/mL
LQFM239 (**8**)	-	500 µg/mL
LQFM240 (**9**)	250 µg/mL	-
LQFM281 (**10**)		250 µg/mL
LQFM282 (**11**)	-	250 µg/mL

3.4. Assessment of Antimycobacterial Activity and Determination of MIC and MBC in Mycobacterium species

The MIC assay of compound LQFM 238 (**7**) against *Mycobacterium* species was shown in Table 3. The MBC of compound LQFM238 (**7**) was further evaluated against *M. abscessus* subsp. *massiliense* strain GO06, Fig. 2. Complete bacterial eradication was observed at an MBC of 1000 µg/mL. At concentrations of 500, 250, 125, 62.5, and 31.25 µg/mL, the corresponding inhibition rates were 81.82%, 70.45%, 29.55%, 11.36%, and 9.09%, respectively.

Table 3
MIC and SI of LQFM238 (**7**) against different mycobacteria strains.

Strain	MIC LQFM238 (µg/mL)	CC50 (µg/mL)	SI[a]
M. avium clinical strain	25	103.80 ± 40.26	4.15
M. abscessus subsp. *bolletii* clinical strain	50	103.80 ± 40.26	2.08
M. abscessus subsp. *abscessus* clinical strain	50	103.80 ± 40.26	2.08
M. tuberculosis - H37Ra ATCC 25177	62,5	103.80 ± 40.26	1.66
M. intracellulare clinical strain	≥ 100	103.80 ± 40.26	-

[a]SI, selectivity index = CC_{50}/MIC

3.5. Morphological Characterization of NTM by SEM

Colonies of *M. abscessus* subsp. *massiliense* GO06 grown on nutrient agar were exposed to LQFM238 (**7**) and examined using SEM. A Fig. 3 illustrated treatment resulted in subtle changes in bacillary thickness and length relative to untreated controls. Control cells exhibited an average thickness of 0.271 µm and a length of 1.889 µm, whereas treated cells showed an average thickness of 0.316 µm and a length of 1.656 µm. The most notable alterations were observed in surface morphology, with treated bacilli displaying a roughened and crumpled appearance compared to the smooth surfaces of control cells.

Legend: **A-** Colonies of *M. abscessus* subsp. *massiliense* GO06 grown on nutrient agar, untreated (control). **B** – SEM analysis of mycobacterial cells exposed to LQFM238 (**7**) at 500 µg/mL for 24 h. Treatment with LQFM238 (**7**) resulted in a roughened surface, giving the bacilli a crumpled appearance. Panels **C** and **D** show minor alterations in bacillary dimensions.

3.6. Cytotoxicity Assay

For a compound to be considered a potential antimicrobial, it must not only exhibit activity against bacterial strains but also demonstrate safety for use in humans and animals. Accordingly, a preliminary cytotoxicity assessment of LQFM238 (**7**) was performed using L929 fibroblast cell line, a standard model in toxicology studies (supplementary data). Toxic effects were observed only at the maximum concentration evaluated (41.67 µg/mL), which showed a statistically significant reduction in cell viability compared to the untreated control (0 µg/mL, $p = 0.0005$), Fig. 4. In addition, to ensure that cytotoxicity was not affected by the solvent, the highest concentration led to markedly higher cell mortality than the DMSO control group ($p = 0.0002$). Lower concentrations (2.6–20.84 µg/mL) had no impact on cell

viability, showing no statistically significant variation relative to the untreated control ($p > 0.9587$) or the DMSO group ($p > 0.8035$). The CC50 of LQFM238 (**7**) was determined to be 103.79 ± 40.25 µg/mL.

3.7. Selectivity index (SI)

The cytotoxicity of the LQFM238 (**7**) was evaluated in L929 fibroblast cells, yielding a CC_{50} of 103.80 ± 40.26 µg/mL. Based on the MIC values obtained, the selectivity index (SI) was 1.66 for *M. tuberculosis* (MIC = 62.5 µg/mL), 2.08 for *M. abscessus* subsp. *abscessus* and *M. abscessus* subsp. *bolletii* (MIC = 50 µg/mL) and 4.15 for *M. avium* (MIC = 25 µg/mL), Table 3.

4. Discussion

All 2-thio-malonylurea compounds exhibited favorable predicted physicochemical properties. Among the compounds evaluated, LQFM238 (**7**), bearing a 3-chlorophenyl substituent, emerged as the most promising candidate. The presence and positional arrangement of the chlorine substituent may contribute to the biological profile of LQFM238 (**7**), as substituent position can influence the electronic distribution, lipophilicity, steric environment, and molecular dipole moment of aromatic compounds, potentially affecting their interactions with bacterial cell-envelope components or intracellular molecular targets. In this context, the meta orientation of the chlorine substituent may provide a distinct balance between electronic and steric effects compared with the corresponding ortho- or para-substituted analogues (Burns et al. 2020; Verma et al. 2023).

In the present study, the 2-thio-malonylurea derivatives exhibited moderate antibacterial activity against the tested Gram-positive bacteria, with MIC values ranging from 125 to 250 µg/mL against *S. aureus* and 250 µg/mL against *E. faecalis*. The selective antibacterial profile observed among compounds **2–11** suggests that small structural modifications within the 2-thio-malonylurea scaffold influence antibacterial activity. Previous studies have also demonstrated the antibacterial activity of thiobarbituric acid-derived Spiro heterocyclic compounds. Kaur et al. (2014) synthesized a series of substituted diphenyl-2,4,8,10-tetraazaspiro[5.5] undecane thiobarbiturate derivatives and evaluated their antibacterial activity against both Gram-positive and Gram-negative bacteria, including *S. aureus* (Kaur et al. 2014). This study is particularly relevant to the present work because these compounds share important structural features with the spirocyclic thiobarbiturate-related scaffold investigated here.

Similarly, Elshaier et al. (2016) reported pyrazole–thiobarbituric acid derivatives with antibacterial activity against *S. aureus* and *E. faecalis*. Among the compounds evaluated, some derivatives exhibited MIC values as low as 16 µg/mL against these Gram-positive bacteria, demonstrating that incorporation of thiobarbituric acid into heterocyclic scaffolds can generate compounds with relevant antibacterial activity (Elshaier et al. 2016). The antibacterial activity observed for LQFM238 (**7**) is consistent with previous reports describing the antimicrobial potential of sulfur-containing heterocyclic scaffolds (Wenholz et al. 2017).

Although the mechanism of action of LQFM238 (**7**) remains to be established, several biological targets have been investigated for structurally related thiobarbiturate compounds. McKinnie et al. (2014) demonstrated that thiobarbiturate-containing compounds can inhibit L,L-diaminopimelate aminotransferase (DapL), an enzyme involved in the lysine biosynthetic pathway. DapL catalyzes a step in the biosynthesis of meso-diaminopimelate and lysine, metabolites that are relevant to bacterial cell-wall and protein biosynthesis. Importantly, the inhibitory activity of thiobarbiturate compounds differed among DapL orthologs, indicating that structural differences in both the ligand and enzyme may influence susceptibility (McKinnie et al. 2014). The DapL-related findings enzymes involved in lysine biosynthesis as potential antibacterial targets (Muduli et al. 2023), should be interpreted as a mechanistic hypothesis based on structural similarity to previously investigated thiobarbiturate compounds rather than as evidence of a direct molecular interaction. DapL may represent a plausible molecular target for LQFM238 (**7**), although this hypothesis requires further studies.

Notably, LQFM238 (**7**) was the only compound active against both bacterial species and was therefore selected for subsequent evaluation against *Mycobacterium* spp. LQFM238 (**7**) demonstrated promising antimycobacterial activity, particularly against *M. avium* isolate (MIC = 25 µg/mL) and clinical *M. abscessus* strains (MIC = 50 µg/mL). The activity of LQFM238 (**7**) was further supported by the morphological alterations observed by SEM. Compared with untreated controls, mycobacterial cells exposed to LQFM238 (**7**) exhibited marked changes in surface alterations, characterized by a roughened and crumpled appearance. These morphological changes are consistent with possible disturbances in cell-envelope integrity and suggest that the mycobacterial envelope may be affected by exposure to the compound. However, SEM provides morphological evidence and does not, by itself, establish the underlying mechanism of action.

Therefore, additional studies addressing membrane permeability, cell-envelope composition, intracellular targets, and potential interactions with mycobacterial metabolic pathways (Moraes et al. 2015), will be necessary to determine whether cell-envelope disruption represents a primary mechanism of action of LQFM238 (**7**). Despite their close taxonomic relationship, the distinct susceptibility profiles observed for *M. avium* and *M. intracellulare* suggest that subtle species-specific differences may affect compound penetration, intracellular exposure, or target engagement.

The cytotoxicity assay demonstrated the ability of the methodology to distinguish viable from non-viable cells in agreement with previously reported approaches (Vijayaraghavareddy et al. 2017; Gomez-Gutierrez et al. 2021). Treatment of L929 fibroblasts with LQFM238 (**7**) resulted in a CC_{50} value of 103.797 µg/mL. This value was higher than the MICs determined for *M. tuberculosis* H37Ra (62.5 µg/mL), *M. avium* (25 µg/mL), and the clinical *M. abscessus* strains (50 µg/mL). Consequently, LQFM238 (**7**) exhibited the highest selectivity index against *M. avium* (SI = 4.15), followed by the clinical *M. abscessus* strains (SI = 2.08). These findings suggest a degree of preferential activity toward mycobacterial cells relative to L929 fibroblasts. Nevertheless, additional studies using different mammalian cell models and complementary toxicity endpoints are necessary to further characterize the safety profile of LQFM238 (**7**). The marked differences in MIC values among the Mycobacterium species

evaluated suggest that the activity of LQFM238 (**7**) may be influenced by species-specific differences in cell-envelope permeability, efflux capacity, metabolic physiology, and/or the accessibility or conservation of potential molecular targets.

5. Conclusion

In conclusion, the present study investigated the antibacterial effect of LQFM238 (**7**) against Gram-positive and Mycobacterial bacterial. LQFM238 (**7**) demonstrated antibacterial activity against both *S. aureus* and *E. faecalis* and exhibited antimycobacterial activity against clinically relevant *Mycobacterium* species. The highest activity was observed against *M. avium*, with a MIC of 25 µg/mL and a selectivity index of 4.15, followed by clinical *M. abscessus* strains, for which a MIC of 50 µg/mL and a selectivity index of 2.08 were observed preferential activity toward mycobacterial cells compared with L929 fibroblasts. Moreover, the morphological alterations observed by scanning electron microscopy suggest that exposure to LQFM238 (**7**) affects mycobacterial cell morphology and may be associated with disturbances in cell-envelope integrity. Future studies should investigate its molecular targets and mechanism of action, including potential interactions with enzymes involved in essential bacterial metabolic pathways, as well as its activity against a broader panel of clinical isolates and its cytotoxicity in additional mammalian cell models.

Declarations

Conflict of interest statement

The authors declare that they have no conflicts of interest.

Author Contribution

Conflict of interest statement The authors declare that they have no conflicts of interest.Author contributionsRicardo Menegatti designed this project. Ricardo Menegatti, André Kipnis, and Pedro Eduardo A. da Silva supervised this project. Ricardo Menegatti, Antônio S. Machado, and Patrícia C. Moreira performed the chemical synthesis. Ieda M. S. Torres, Glaura R. de C. e C. Lima, Maria Micaella R. Pereira, André Kipnis, Tracy Martina M. Martins, Pedro Eduardo A. da Silva, Ana Julia Reis, and Yasmin C. das Neves was performed biological screening and MIC assays. Vinícius S. Pinto and Luciano M. Lião performed the NMR analysis. André Kipnis, Maria Micaella R. Pereira and Tracy Martina M. Martins performed the SEM analysis. Beatriz S. Gontijo, José R. do Carmo Neto, and Jonathas X. Pereira performed the “Live and dead” assay. All authors analyzed the data and wrote the manuscript.

Acknowledgement

AcknowledgmentsThe authors gratefully acknowledge the Fundação de Apoio à Pesquisa (FUNAPE/UFG), the Programa Nacional de Cooperação Acadêmica (PROCAD), and the Coordenação de Aperfeiçoamento de Pessoal de Nível Superior (CAPES), as well as the Conselho Nacional de Desenvolvimento Científico e Tecnológico (CNPq; process No. 409446/2025-4), for financial support. The authors also thank the Regional Center for Technological Development and Innovation (CRTI) and the High-Resolution Microscopy Multiuser Laboratory (LabMic/UFG) at the Federal University of Goiás for their assistance with electron microscopy. The authors are also grateful to Dr. Boniek Vaz Gontijo for performing the mass spectrometry analyses.

References

1. Burns RJ, Mati IK, Muchowska KB et al (2020) Quantifying Through-Space Substituent Effects. Angew Chemie Int Ed 59:16717–16724. https://doi.org/https://doi.org/10.1002/anie.202006943
2. Clayden J, Greeves N, Warren S, Wothers P (1916) Organic chemistry. J Chem Soc Abstr 110:i197. https://doi.org/10.1039/ca9161000197
3. Clinical and Laboratory Standards Institute (CLSI) (2018) Performance Standards for Antimicrobial Susceptibility Testing: 28th Edition Informational Supplement M100-S27; CLSI: Wayne, PA, USA, 2018
4. da Mota MF, de Carvalho FS, de Ávila RI et al (2018) LQFM030 reduced Ehrlich ascites tumor cell proliferation and VEGF levels. Life Sci 201:1–8. https://doi.org/10.1016/j.lfs.2017.12.029
5. Dabholkar VV, Ravi TD (2010) Synthesis of biginelli products of thiobarbituric acids and their antimicrobial activity. J Serbian Chem Soc 75:1033–1040. https://doi.org/10.2298/JSC090106060D
6. Das Neves RC, Mortari MR, Schwartz EF et al (2019) Antimicrobial and antibiofilm effects of peptides from venom of social wasp and scorpion on multidrug-resistant acinetobacter baumannii. Toxins (Basel) 11:1–18. https://doi.org/10.3390/toxins11040216
7. Elshaier YAMM, Barakat A, Al-Qahtany BM et al (2016) Synthesis of pyrazole-Thiobarbituric acid derivatives: Antimicrobial activity and docking studies. Molecules 21:1–17. https://doi.org/10.3390/molecules21101337
8. Gomez-Gutierrez JG, Bhutiani N, McNally MW et al (2021) The neutral red assay can be used to evaluate cell viability during autophagy or in an acidic microenvironment in vitro. Biotech Histochem 96:302–310. https://doi.org/10.1080/10520295.2020.1802065
9. Guo Y, Cao X, Yu J et al (2020) Antimicrobial susceptibility of Mycobacterium abscessus complex clinical isolates from a Chinese Tertiary Hospital. Infect Drug Resist 13:2001–2010. https://doi.org/10.2147/IDR.S252485
10. Ikuta KS, Swetschinski LR, Robles Aguilar G et al (2022) Global mortality associated with 33 bacterial pathogens in 2019: a systematic analysis for the Global Burden of Disease Study 2019. Lancet 400:2221–2248. https://doi.org/10.1016/S0140-6736(22)02185-7
11. Jin X, Zheng CJ, Song MX et al (2012) Synthesis and antimicrobial evaluation of L-phenylalanine-derived C5-substituted rhodanine and chalcone derivatives containing thiobarbituric acid or 2-

thioxo-4-thiazolidinone. Eur J Med Chem 56:203–209. https://doi.org/10.1016/j.ejmech.2012.08.026

12. Kaur G, Gupta P, Harjai K, Singh V (2014) Synthesis of new thiobarbituric acid derived spiroheterobicyclic compounds and their antimicrobial activity. Drug Dev Res 75:202–210. https://doi.org/10.1002/ddr.21172
13. Lamut A, Peterlin Mašič L, Kikelj D, Tomašič T (2019) Efflux pump inhibitors of clinically relevant multidrug resistant bacteria. Med Res Rev 39:2460–2504. https://doi.org/10.1002/med.21591
14. Langford BJ, Soucy J-PR, Leung V et al (2023) Antibiotic resistance associated with the COVID-19 pandemic: a systematic review and meta-analysis. Clin Microbiol Infect Off Publ Eur Soc Clin Microbiol Infect Dis 29:302–309. https://doi.org/10.1016/j.cmi.2022.12.006
15. Lou B, Chen Z-Q, Bian Z-Q, Huang C-H (2010) Multisignaling detection of cyanide anions based on an iridium (III) complex: remarkable enhancement of sensitivity by coordination effect. New J Chem 34:132–136
16. Martin A, Camacho M, Palomino JC (2003) Resazurin Microtiter Assay Plate Testing of Mycobacterium tuberculosis Susceptibilities to Second-Line Drugs: Rapid, Simple, and Inexpensive Method. Antimicrob Agents Chemother 47:3616–3619. https://doi.org/10.1128/AAC.47.11.3616
17. Martins TMM, Lião LM, Oliveira GAR et al (2025) In Vitro Antimycobacterial Activity Evaluation of a New Lead Compound (LQFM326) against Clinical Strains of Mycobacterium sp. ACS Omega 10:39875–39883. https://doi.org/10.1021/acsomega.5c04174
18. McKinnie SMK, Rodriguez-Lopez EM, Vederas JC et al (2014) Differential response of orthologous l,l-diaminopimelate aminotransferases (DapL) to enzyme inhibitory antibiotic lead compounds. Bioorg Med Chem 22:523–530. https://doi.org/10.1016/j.bmc.2013.10.055
19. Moraes GL, Gomes GC, Monteiro de Sousa PR et al (2015) Structural and functional features of enzymes of Mycobacterium tuberculosis peptidoglycan biosynthesis as targets for drug development. Tuberculosis (Edinb) 95:95–111. https://doi.org/10.1016/j.tube.2015.01.006
20. Muduli S, Karmakar S, Mishra S (2023) The coordinated action of the enzymes in the L-lysine biosynthetic pathway and how to inhibit it for antibiotic targets. Biochim Biophys Acta - Gen Subj 1867:130320. https://doi.org/10.1016/j.bbagen.2023.130320
21. Murray CJL, Ikuta KS, Sharara F et al (2022) Global burden of bacterial antimicrobial resistance in 2019: a systematic analysis. Lancet 399:629–655. https://doi.org/10.1016/S0140-6736(21)02724-0
22. NCCLS (2003) Methods for Dilution Antimicrobial Susceptibility Tests for Bacteria That Grow Aerobically; Approved Standard—Sixth Edition - NCCLS document M7-A6
23. Oliveira FM, Da Costa AC, Procopio VO et al (2018) Mycobacterium abscessus subsp. massiliense mycma_0076 and mycma_0077 genes code for ferritins that are modulated by iron concentration. Front Microbiol 9:1–16. https://doi.org/10.3389/fmicb.2018.01072
24. Palomino J-C, Martin A, Camacho M et al (2002) Resazurin microtiter assay plate: simple and inexpensive method for detection of drug resistance in Mycobacterium tuberculosis. Antimicrob Agents Chemother 46:2720–2722. https://doi.org/10.1128/AAC.46.8.2720-2722.2002

25. Raiol T, Ribeiro GM, Maranhão AQ et al (2012) Complete genome sequence of Mycobacterium massiliense. J Bacteriol 194:5455. https://doi.org/10.1128/JB.01219-12
26. Ramis IB, Cnockaert M, von Groll A et al (2015) Antimicrobial susceptibility of rapidly growing mycobacteria using the rapid colorimetric method. Eur J Clin Microbiol Infect Dis Off Publ Eur Soc Clin Microbiol 34:1403–1413. https://doi.org/10.1007/s10096-015-2365-2
27. Repetto G, del Peso A, Zurita JL (2008) Neutral red uptake assay for the estimation of cell viability/cytotoxicity. Nat Protoc 3:1125–1131. https://doi.org/10.1038/nprot.2008.75
28. Shahamirian M, Wieczorkiewicz PA, Krygowski TM, Szatylowicz H (2023) Substituent Effects from the Point of View of Energetics and Molecular Geometry in Acene, Polyene, and Polyyne Derivatives. J Org Chem 88. https://doi.org/https://doi.org/10.1021/acs.joc.2c02936
29. Sharma A, Noki S, Zamisa SJ et al (2018) Exploiting the Thiobarbituric Acid Scaffold for Antibacterial Activity. ChemMedChem 13:1923–1930. https://doi.org/10.1002/cmdc.201800414
30. Verma C, Alfantazi A, Quraishi MA, Rhee KY (2023) Significance of Hammett and Taft substituent constants on bonding potential of organic corrosion inhibitors: Tailoring of reactivity and performance. Coord Chem Rev 495:215385. https://doi.org/https://doi.org/10.1016/j.ccr.2023.215385
31. Vijayaraghavareddy P, Adhinarayanreddy V, Vemanna RS et al (2017) Quantification of Membrane Damage/Cell Death Using Evan's Blue Staining Technique. Bio-protocol 7:e2519. https://doi.org/10.21769/BioProtoc.2519
32. Wang C, Shi Y, Yang B et al (2026) Comorbidity profiles of non-tuberculous mycobacteria infections in China: 12 years' experience. https://doi.org/https://doi.org/10.1128/spectrum.02018-25. Microbiol Spectr 14:
33. Wenholz DS, Zeng M, Ma C et al (2017) Small molecule inhibitors of bacterial transcription complex formation. Bioorg Med Chem Lett 27:4302–4308. https://doi.org/https://doi.org/10.1016/j.bmcl.2017.08.036
34. Wiegand I, Hilpert K, Hancock REW (2008) Agar and broth dilution methods to determine the minimal inhibitory concentration (MIC) of antimicrobial substances. Nat Protoc 3:163–175. https://doi.org/10.1038/nprot.2007.521

Figures

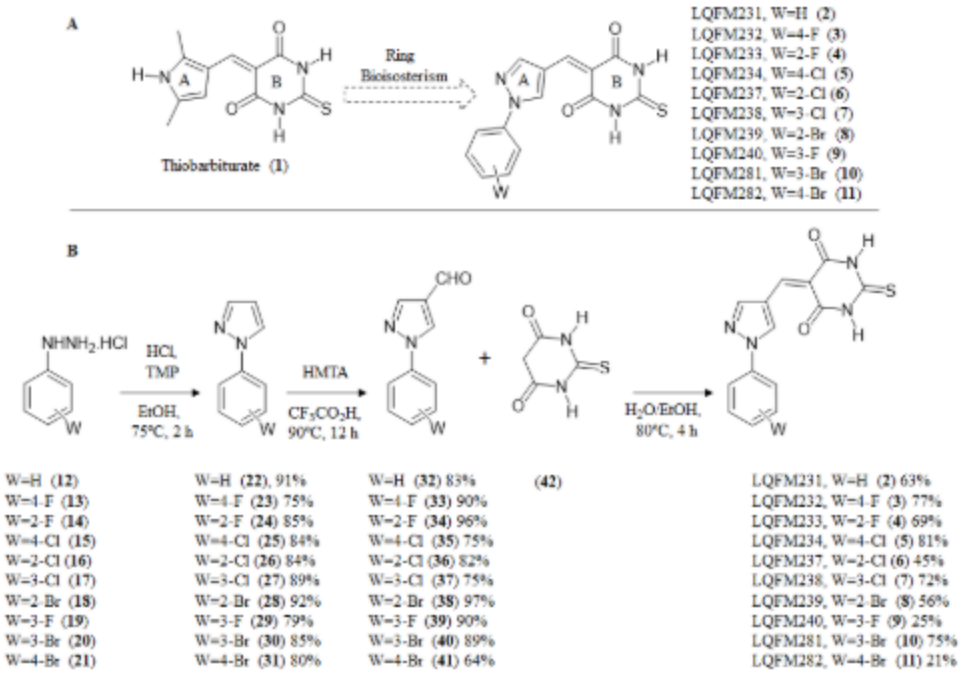


Figure 1

1A - Structure, Design, and Synthesis of LQFM Compounds Based on 2-tio-malonilureia Scaffolds (1-42);
1B - Synthetic route for the preparation of LQFMs (compounds 2-11).

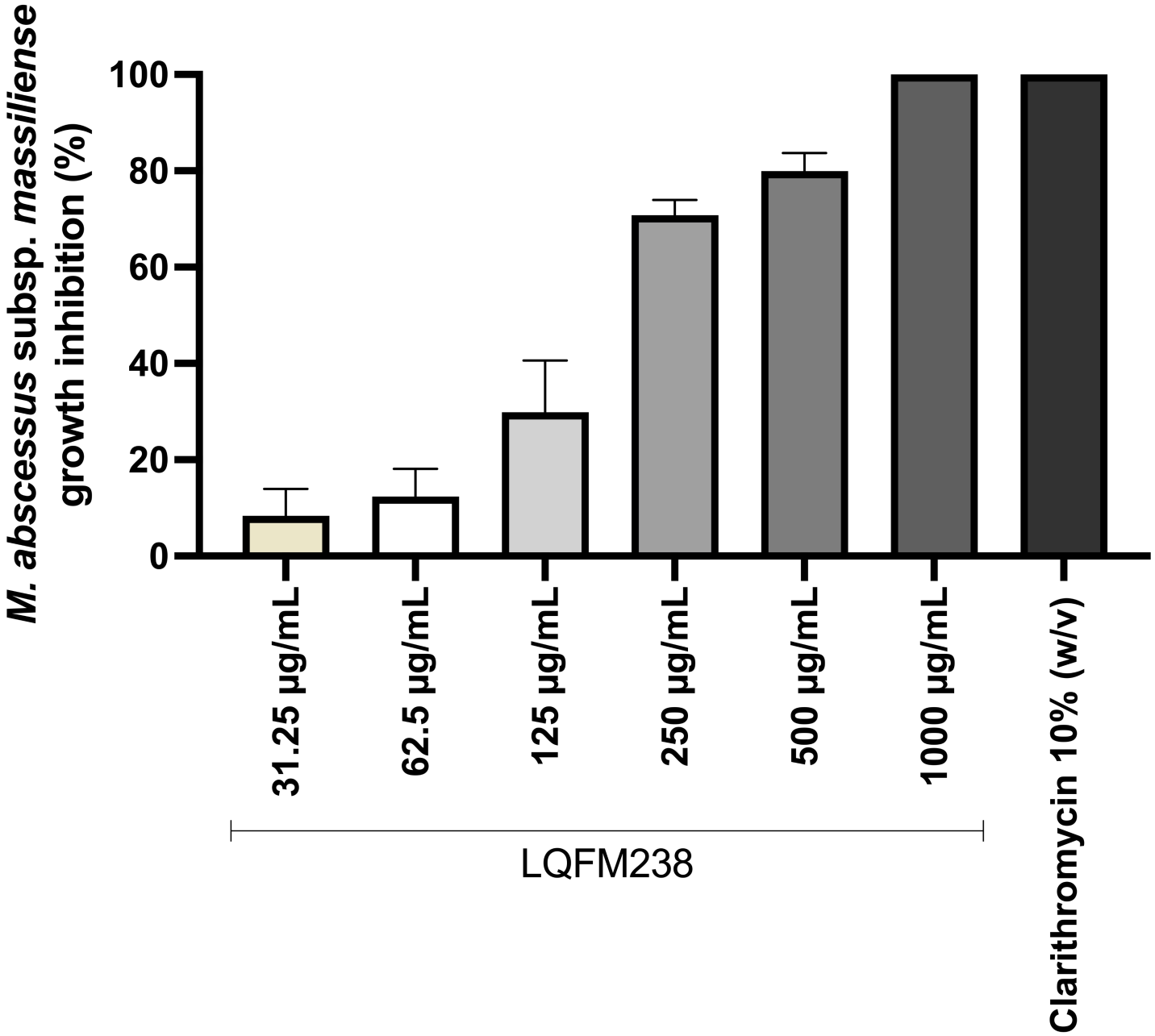


Figure 2

MBC of compound LQFM238 (**7**).

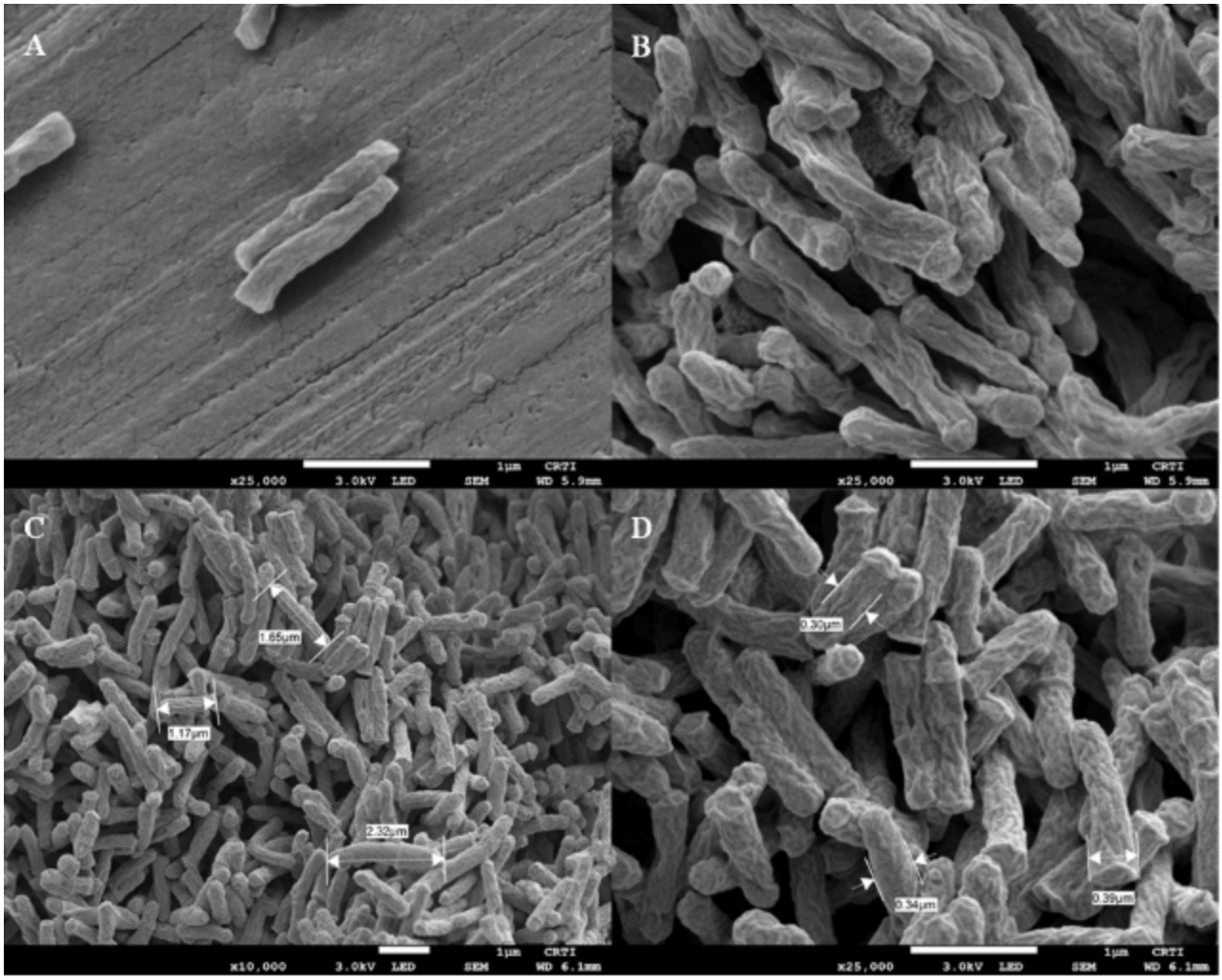


Figure 3

SEM analysis of mycobacterial cells exposed to LQFM238 (**7**) for 24h.

Legend: **A-** Colonies of *M. abscessus* subsp. *massiliense* GO06 grown on nutrient agar, untreated (control). **B** – SEM analysis of mycobacterial cells exposed to LQFM238 (**7**) at 500 µg/mL for 24 h. Treatment with LQFM238 (**7**) resulted in a roughened surface, giving the bacilli a crumpled appearance. Panels **C** and **D** show minor alterations in bacillary dimensions.

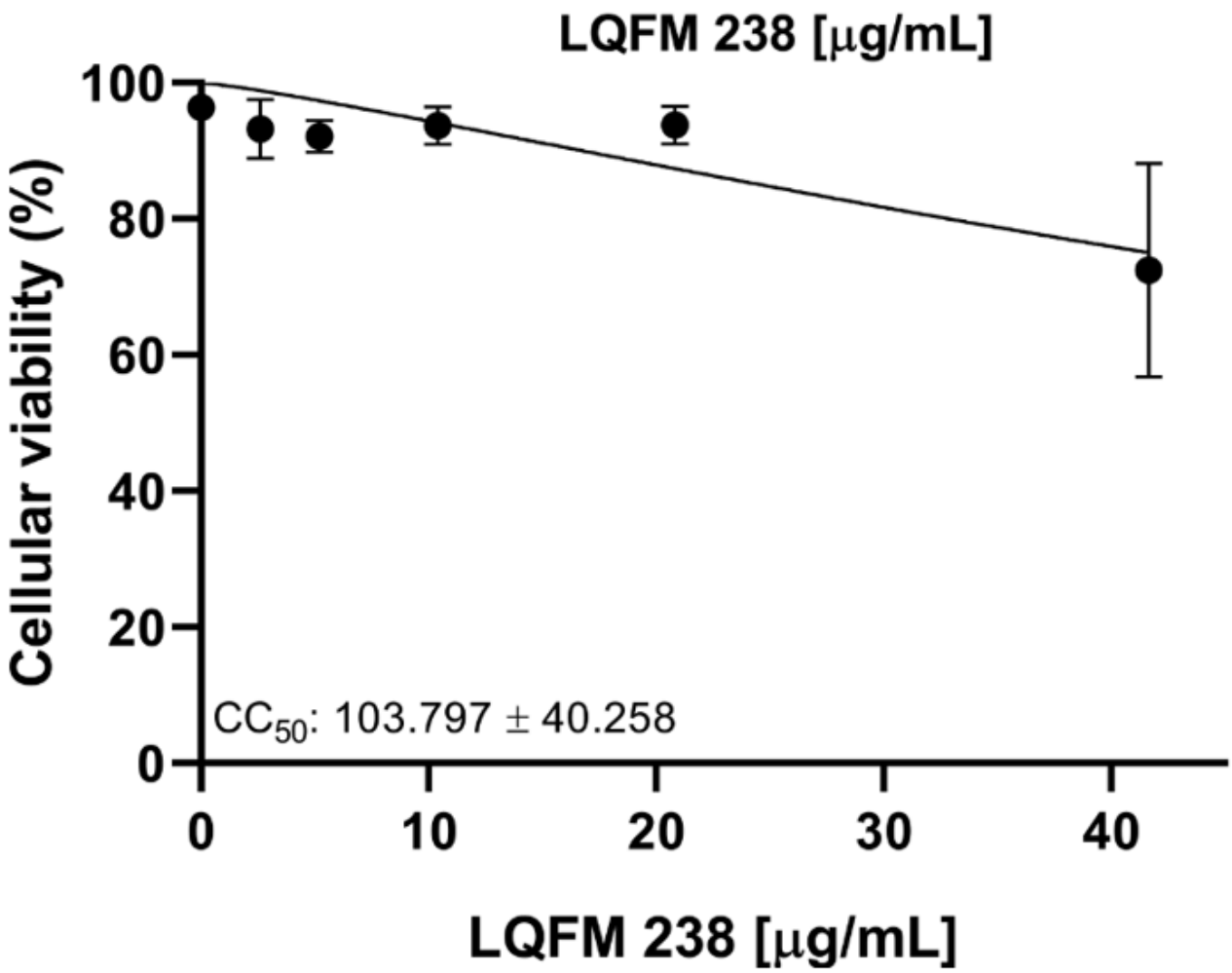


Figure 4

CC50 curve after exposure to LQFM238 (**7**)

Supplementary Files

This is a list of supplementary files associated with this preprint. Click to download.

- SupplementarydataMoreiraetal.2026.docx